Comparison of Kifunensine and 1-Deoxymannojirimycin Binding to Class I and II α-Mannosidases Demonstrates Different Saccharide Distortions in Inverting and Retaining Catalytic Mechanisms[†,‡]

Niket Shah,[§] Douglas A. Kuntz,[||] and David R. Rose*[,§,||]

Department of Medical Biophysics, University of Toronto, and Division of Molecular and Structural Biology, Ontario Cancer Institute, Princess Margaret Hospital, 610 University Avenue, Room 7-113, Toronto, Ontario, Canada M5G 2M9

Received May 7, 2003; Revised Manuscript Received October 2, 2003

ABSTRACT: Mannosidases are key enzymes in the eukaryotic N-glycosylation pathway. These enzymes fall into two broad classes (I and II) and are characteristically different in catalytic mechanism, sequence, and structure. Kifunensine is an alkaloid that is a strong inhibitor against class I α-mannosidases but is only a weak inhibitor against class II α-mannosidases. In this paper, the 1.80 Å resolution crystal structure of kifunensine bound to *Drosophila melanogaster* Golgi α-mannosidase II (dGMII) is presented. Kifunensine adopts a $^{1,4}B$ boat conformation in the class II dGMII, which contrasts the $^{1}C_4$ chair conformation seen in class I human endoplasmic reticulum α1,2 mannosidase (hERMI, PDB 1FO2). The observed conformations are higher in conformational energy than the global minimum $^{4}C_1$ conformation, although the conformation in hERMI is closer to the minimum, as supported by an energy calculation. Differing conformations of 1-deoxymannojirimycin were also observed: a $^{4}C_1$ and $^{1}C_4$ conformation in dGMII and hERMI, respectively. Thus, these two α-mannosidase classes distort these inhibitors in distinct manners. This is likely indicative of the binding characteristics of the two different catalytic mechanisms of these enzymes.

The eukaryotic N-glycosylation pathway is responsible for the conjugation of oligosaccharides to specific asparagine residues in nascent proteins. Several diseases result from malfunctions in the N-glycosylation pathway, including neurological disorders and storage diseases of the lysosome (*1*−*3*). In certain cancers, there is an unusual distribution of oligosaccharides on the tumor cell surface whose presence has been hypothesized to allow the tumor cell to evade components of the immune system, such as carbohydrate-mediated recognition (*1*, *4*, *5*).

The process of N-glycosylation consists of successive steps of extension and trimming by a variety of enzymes. At the outset, a lipid-linked sugar precursor is transferred to the asparagine residue of the N-glycosylation sequon (Asn-*X*-Ser/Thr, where $X \neq$ Pro) of the nascent protein in the endoplasmic reticulum (ER).[1] This is followed by a series of trimming steps by glucosidases and α-mannosidases. The glycosylated protein is then transported to the *cis*-Golgi apparatus where there are a series of trimming and elongation steps by a variety of glycosyl hydrolases and glycosyl transferases as the maturing glycoprotein travels through the *cis*-, *medial*-, and *trans*-Golgi apparatus. The protein is then secreted from the Golgi en route to its final destination. This process has recently been reviewed in ref *6*.

α-Mannosidases remove mannose residues from the maturing oligosaccharide by hydrolyzing the mannosyl glycosidic bond. These enzymes fall into two categories, class I and class II, based primarily on sequence similarity and preferred substrates (Table 1) (*7*). Since the two classes differ in product stereochemistry, bond specificity and inhibitor structure, it can be surmised that their catalytic mechanisms are different, and inverting and retaining mechanisms have been proposed for each class.

The class I ER α1,2-mannosidase (mannosyl-oligosaccharide 1,2-α-mannosidase, EC 3.2.1.113) catalyzes the removal of a single α1,2 linked mannose from $Man_9GlcNAc_2$, producing $Man_8GlcNAc_2$ (*7*). This enzyme is involved in the degradation of misfolded proteins in the cell, as the trimming of a single mannose at this step is a targeting signal for translocation out of the ER to the proteasome for degradation (*7*). The atomic structure of the human enzyme was published by Howell et al. (PDB accession codes: 1FM1, 1FO2, and 1FO3) (*7*, *12*).

Golgi α-mannosidase II (mannosyl-oligosaccharide 1,3-1,6-α-mannosidase, EC 3.2.1.114) is a class II α-mannosidase in the N-glycosylation pathway that catalyzes the hydrolysis of the terminal α1,3- and α1,6-linked mannoses in the high-mannose oligosaccharide $GlcNAcMan_5GlcNAc_2$,

[†] N.S. received funding through a postgraduate scholarship from the Natural Sciences and Engineering Research Council of Canada (NSERC). This work was supported by a grant from the Canadian Institutes for Health Research (CIHR).

[‡] The PDB accession number for the structure presented in this paper is 1PS3.

* Corresponding author. Phone: (416) 946-2970. Fax: (416) 946-6529. E-mail: drose@uhnres.utoronto.ca.

[§] University of Toronto.

[||] Ontario Cancer Institute.

[1] Abbreviations: dGMII, *Drosophila melanogaster* Golgi α-mannosidase II; DMJ, 1-deoxymannojirimycin; ER, endoplasmic reticulum; GlcNAc, *N*-acetylglucosamine; hERMI, human endoplasmic reticulum α1,2 mannosidase; KIF, kifunensine; Man, mannose.

10.1021/bi034742r CCC: $25.00
Published on Web 11/07/2003

Table 1: Comparison of Class I and II α-Mannosidases[a]

	class I	class II
glycosyl hydrolase classification	family 47	family 38
metal ion dependence	Ca^{2+}	Zn^{2+}, Co^{2+}
topology	type II TM	type II TM
mannose linkages hydrolyzed	α1,2	α1,2; α1,3; α1,6
stereochemistry of product	inverted	retained
optimal inhibitors	pyranose analogues	furanose analogues

[a] Adapted from ref *7*.

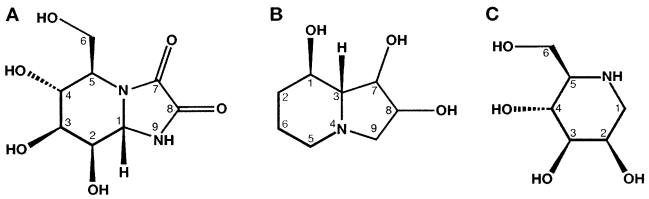

FIGURE 1: Chemical structures of the inhibitors examined in this paper. (A) Kifunensine, (B) swainsonine, and (C) 1-deoxymannojirimycin; abbreviated KIF, SWA, and DMJ, respectively. The ring numbering schemes are taken from the following structures: PDB 1FO3 (KIF), 1HWW (SWA), and 1FO2 (DMJ) (*9*, *17*).

converting it to *GlcNAcMan*$_3$*GlcNAc*$_2$ (*8*, *9*). The cleavage of these two bonds is the committed step of complex *N*-glycan formation (*10*). The structure of Golgi α-mannosidase II from *Drosophila melanogaster* (dGMII) has been solved, and several inferences as to putative catalytic residues have been made (PDB 1HTY, 1HWW, and 1HXK) (*9*). Recently, a second class II α-mannosidase structure, that of the bovine lysosomal enzyme, was published and suggested an intriguing low pH activation mechanism for that enzyme (PDB 1O7D) (*11*).

Kifunensine (Figure 1) is an alkaloid that is a cyclic oxamide derivative of 1-aminodeoxymannojirimycin and is produced by the actinomycete *Kitasatosporia kifunense* 9482 (*13*). Kifunensine is a highly specific inhibitor of class I α-mannosidases and inhibits these enzymes from plant and rat with IC_{50} values of 20−50 and 100 nM, respectively (*13*, *14*). However, the inhibition of class II α-mannosidases is much weaker with an IC_{50} value of 120 μM for Jack bean α-mannosidase (*13*) and a K_i value of 5.2 mM for *Drosophila* Golgi α-mannosidase II (this paper).

1-Deoxymannojirimycin (DMJ) is a mannose analogue with a nitrogen at the typical ring oxygen position. DMJ is a somewhat efficacious inhibitor against both class I and class II α-mannosidases, and structures of DMJ in complex with both hERMI and dGMII have been solved to high resolution (*9*, *12*).

Here, we present the structure of kifunensine, a weak class II α-mannosidase inhibitor, bound to dGMII, a class II α-mannosidase. The low efficacy of kifunensine against dGMII versus its efficacy against hERMI is examined from a structural perspective. For comparative purposes, 1-deoxymannojirimycin binding is also examined in both enzymes.

MATERIALS AND METHODS

Inhibition Assay. Inhibition of α-mannosidase activity was carried out in microtiter plates in a final volume of 50 μL. Inhibitors were dissolved in water to a final concentration of 200 mM. The reaction mixture consisted of 25 μL of varying concentrations (1−10 mM) *p*-nitrophenol-α mannoside (*p*-NP-mannose) from Sigma, 10 μL of 200 mM buffer, and 10 μL of water or inhibitor. The buffer used was MES pH 5.75, which is optimal for this enzyme (*8*). The reaction mixture was pre-warmed to 37 °C, and 5 μL of α-mannosidase in 10 mM sodium phosphate pH 6.8, 100 mM NaCl is added to initiate the reaction. The amount of enzyme added was that which is necessary to keep the reaction in the linear range. This represented approximately 350 ng of protein for a 15 min reaction. At the endpoint, the reaction was stopped using 50 μL of 0.5 M sodium carbonate. The absorbance of the reaction was measured at 405 nm with 520 nm background correction on a micotiter plate reader. The measurements were taken in the absence and presence of each inhibitor to determine Michaelis−Menten kinetics. K_i values were derived from the *x*-intercepts of the double reciprocal plots.

Crystallization. Crystallization of dGMII was carried out as described in ref *9*. A total of 2 μL of concentrated protein solution was combined with 2 μL of reservoir buffer (100 mM Tris pH 7, 8.5% PEG 6000, 2.5% methyl-pentanediol) to form the crystallization drop. After 16−18 h of growth, the crystals were ready to be exposed to inhibitor.

Inhibitor Addition and Freezing. The crystals were washed in phosphate reservoir buffer: 100 mM sodium phosphate pH 7, 8.5% PEG 6000, 2.5% MPD. Kifunensine was added in phosphate reservoir buffer at 10 mM concentration. Three 2 μL additions of kifunensine were added to the crystal drop, each one followed by a removal of 2 μL of solution from the drop. Each addition and removal step was followed by a soak time of approximately 30 min. The overall effect of this technique was to reduce the Tris concentration in the drop while simultaneously increasing the kifunensine concentration.

The crystals were then removed from the hanging drop and exposed to phosphate reservoir buffer + kifunensine with increasing concentrations of MPD (5−20%) and flash-frozen in a nitrogen stream. They were tested for preliminary diffraction and then stored in liquid nitrogen for transport to the X-ray source.

Data Collection. The crystals were exposed to X-ray radiation in beam-line F1 at the Cornell High Energy Synchrotron Source (CHESS) at Cornell University in Ithaca, NY. Data were collected using dual ADSC Quantum-4 CCD detectors. *DENZO* and *SCALEPACK* were used to process the data (*15*). Final reduction statistics are presented in Table 2.

Structure Determination. The previously solved structure of dGMII was used in conjunction with the collected data to generate σ_a-weighted difference maps ($F_o - F_c$) using CNS (*16*). These maps unambiguously showed the position and orientation of the kifunensine in the active site (Figure 2). The electron density maps were verified from a second independently grown and treated crystal.

Energy Calculations. The coordinates of the inhibitor alone were removed from the associated enzyme and were subjected to a molecular dynamics simulation using the *DISCOVER* suite in *InsightII* ($n_{equilibration} = 100$, $n_{steps} = 1000$, $n_{history} = 10$). The resulting energy values in kcal/mol are reported in Table 4.

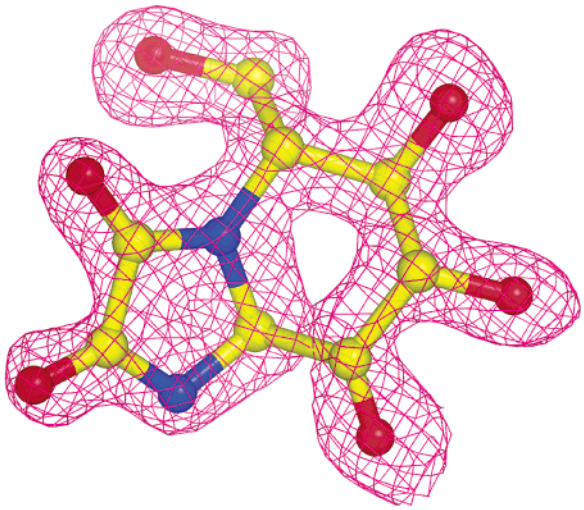

FIGURE 2: Electron density of kifunensine in the dGMII active site. The σ_A-weighted unbiased difference density ($2F_o - F_c$) is presented to 1.80 Å resolution and was contoured to 1.0σ (0.44 electrons/Å^3). This density was calculated before inclusion of the inhibitor in the calculations.

Table 2: Data Reduction and Refinement Statistics for dGMII·KIF[a]

wavelength (Å)	0.9504
temperature (K)	100
resolution range (Å)	30−1.80
highest resolution shell (Å)	1.83−1.80
mosaicity	0.601
completeness (overall/highest shell)	94.2/83.3%
I/σ_I (overall/highest shell)	16.3/4.1
R_{merge} (overall/highest shell)	0.058/0.180
reflections (total/unique)	759620/144642
redundancy	5.25
R_{cryst}	0.200
R_{free}	0.222
atoms	9205
residues	1014
water molecules	986
RMSD bonds (Å)	0.0058
RMSD angles (deg)	1.34
average *B*-factors for protein (Å^2)	13.66
average *B*-factors for inhibitor atoms (Å^2)	17.81

[a] *R*-factor = $(\Sigma||F_o| - |F_c||)/(\Sigma|F_o|)$.

RESULTS

Inhibition of dGMII. We found that kifunensine was a weak inhibitor of dGMII, with a K_i value of 5.2 mM against dGMII. By comparison, the K_i for swainsonine was much lower at 10.5 nM in identical conditions.

Obtaining a Crystal Complex. Initial cocrystal trials failed to show the presence of kifunensine in the active site. Instead, the observed density could only be attributed to a Tris molecule. The presence of Tris in the active site was previously seen in the dGMII structure (ref *9*, PDB 1HTY) and in the lysosomal α-mannosidase structure (ref *11*, PDB 1O7D). Because of the presence of this interfering Tris molecule, we then attempted to grow crystals in the presence of phosphate. Although we could produce large, prismatic crystals in this manner, they failed to diffract beyond about 7 Å. We thus resorted to removing the bound Tris by soaking the molecules in a solution based on the mother liquor with the Tris replaced by sodium phosphate. Initial crystallographic studies of these phosphate-soaked crystals indicated the absence of clear Tris density in the active site, so kifunensine was added to phosphate-washed crystals. Kifunensine was also added to the solutions used for cryoprotection prior to freezing to prevent the loss, by dilution, of this weakly bound substrate. Kifunensine-soaked dGMII crystals were assessed for quality on our home X-ray source, and those with the best diffraction and lowest mosaicity were analyzed on the F1 line at CHESS. Data sets to 1.8 Å resolution were collected from two crystals, although some diffraction was observable beyond that limit.

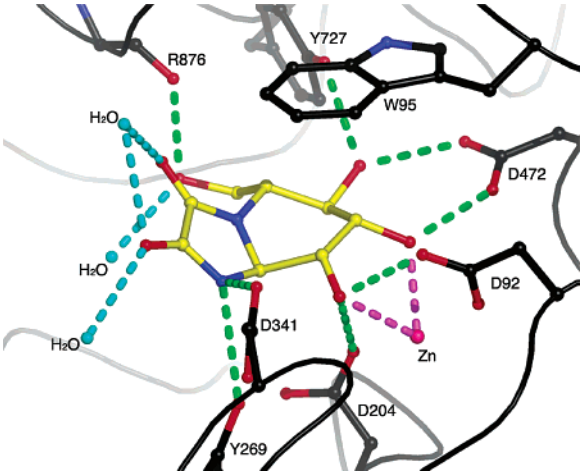

FIGURE 3: Kifunensine in the dGMII active site. There are many KIF-residue interactions, including hydrogen bonding (green and cyan dashes), metal coordination (violet dashes), and stacking with aromatic side chain of W95.

Table 3: Atomic Interactions of dGMII with Kifunensine, Swainsonine, and 1-Deoxymannojirimycin (KIF, SWA, and DMJ, respectively)[a]

dGMII	KIF	distance	SWA	distance	DMJ	distance
D204OD1	O_2H	2.92	N_4	2.88	O_2H	2.75
D341OD2	N_9	2.74				
D472OD1	O_4H	2.61	O_1H	2.51	O_4H	2.80
D472OD2	O_3H	2.37	O_7H	2.61		
D92OD1	O_2H	2.75	O_8H	2.91	O_3H	2.90
R876O	O_6H	2.76			O_6H	2.60
Y269OH	N_9	3.00				
Y727OH	O_4H	2.72	O_1H	2.69		
Zn	O_2H	2.41	O_7H	2.31	O_2H	2.41
	O_3H	2.37	O_8H	2.30	O_3H	2.33
K_i	5.2 mM		10.5 nM		610 μM	

[a] All distances shown are in Å.

Kifunensine·dGMII Complex. The kifunensine binds to dGMII in the active site (Figure 2) and is stabilized by interactions with a variety of residues. The 2- and 3-hydroxyl groups on the pyranosyl portion of kifunensine (Figure 1) coordinate the zinc ion at the active site. The six-membered ring of kifunensine stacks against Trp95 of the enzyme, with Trp415 stacking against the C5−C6−C7 portion of the inhibitor (Figure 3). There are many inhibitor−enzyme interactions, including hydrogen bonds with putative catalytic residues Asp204, Asp341, and Asp472. These and other interactions are summarized in Table 3 and Figure 4. The mode of binding is similar to the extremely efficacious class II α-mannosidase inhibitor swainsonine (Figure 5), whose 2- and 3-hydroxyl groups on the furanose ring also coordinate the zinc ion, and similar stacking and hydrogen bonding interactions are also seen (*9*). The pyranose portion of kifunensine adopts a $^{1,4}B$ boat conformation in the dGMII

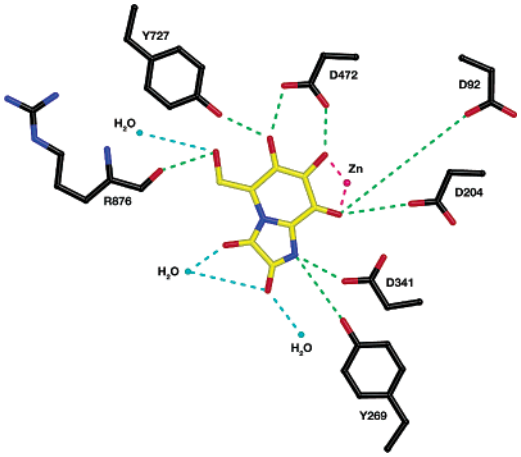

FIGURE 4: KIF·dGMII interactions. The interactions shown are ≤3 Å in distance. There are additional stacking interactions with aromatic side chains that are not shown (see text).

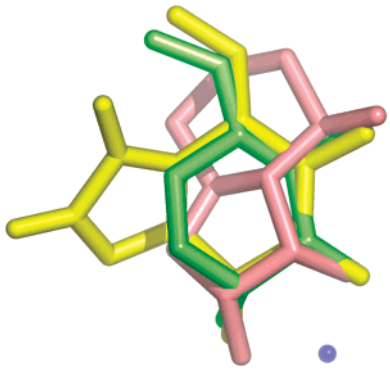

FIGURE 5: Superposition of inhibitors in dGMII active site. The molecules shown are kifunensine (yellow), 1-deoxymannojirimycin (green), swainsonine (salmon), and the dGMII active site zinc (indigo). These molecules represent a range of dGMII inhibition over 4 orders of magnitude.

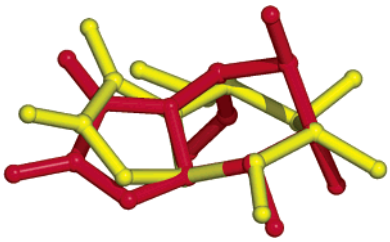

FIGURE 6: Superposition of kifunensine from two α-mannosidases: dGMII (yellow) and hERMI (red). It is evident that kifunensine is in two distinct conformations in each enzyme: $^{1,4}B$ in dGMII and $^{1}C_4$ in hERMI. In addition, there is an all-equatorial conformation for the pyranose ring hydroxyls in dGMII, as contrasted to an all-axial conformation in hERMI.

active site and has a prominent kink along the C_1-N bond. The kifunensine ring hydroxyls adopt an all-equatorial conformation, which contrasts the all-axial conformation seen in hERMI (Figure 6) (*12*).

Kifunensine Energy. The total energy of kifunensine (the sum of potential and kinetic energies) was calculated to be 101.46 kcal/mol in dGMII as compared to 97.59 kcal/mol in hERMI (Table 4). This difference of 4 kcal/mol may be attributed to the kinked conformation that kifunensine adopts in the dGMII active site, as opposed to the planar conformation in hERMI. The energy difference cannot be attributed to protein−inhibitor interactions, as the energy calculation was performed on kifunensine isolated from the active sites of the two enzymes.

Table 4: KIF Energies (kcal/mol)

	isolated from hERMI	isolated from dGMII
total energy	97.590 ± 2.060	101.457 ± 0.987
potential energy	73.073 ± 3.000	76.413 ± 2.881
kinetic energy	24.518 ± 2.767	25.044 ± 2.758

DISCUSSION

Comparison of Kifunensine in dGMII and hERMI. Kifunensine forms similar interactions in both dGMII and hERMI as a considerable number of hydrogen bonds are seen between amino acid residues and ring hydroxyls, as well as stacking interactions with aromatic side chains. However, biochemical assays have shown that kifunensine is a strong inhibitor of class I α-mannosidases but is rather ineffective against class II α-mannosidases, including dGMII. The details of the kifunensine in the dGMII active site may indicate what features make kifunensine a poor inhibitor in class II α-mannosidases.

Kifunensine binds to both dGMII and hERMI in nonstandard conformations (Figure 6). The conformation of kifunensine in the KIF·hERMI complex is a $^{1}C_4$ chair conformation, with an all-axial configuration of ring hydroxyls (*17*). It is hypothesized that this all-axial conformation exists due to the presence of the fused five-membered ring to the pyranosyl portion of kifunensine. Neither the $^{1}C_4$ conformation in hERMI nor the $^{1,4}B$ conformation in dGMII represent the accepted low energy state for mannose derivatives, which is $^{4}C_1$ (*18*). However, the $^{1}C_4$ conformation has been shown to be of a lower energy than $^{1,4}B$ and thus closer to the expected global minimum of $^{4}C_1$ (*19*). This is supported by the energy calculations presented in this paper, which show a 4 kcal/mol increase in energy between the hERMI- and dGMII-bound kifunensine forms.

dGMII Inhibitor Comparison. High-resolution crystal structures of dGMII complexes with swainsonine, 1-deoxymannojirimycin, and kifunensine have been solved (*9*). This represents a span of dGMII inhibitor constants over 4 orders of magnitude.

The comparison of kifunensine, 1-deoxymannojirimycin, and swainsonine in dGMII demonstrates the similarity of metal coordination (Figure 5). The zinc coordination distances and geometry are very similar for each inhibitor in dGMII, as well as the interactions with various protein side chains and the backbone (Table 3). It is interesting to note that the weakest inhibitor, kifunensine, is oriented so that it occupies a region of the active site shown to be unoccupied in dGMII·DMJ and dGMII·swainsonine. This may indicate that there are unfavorable interactions taking place in that part of the active site, reducing the efficacy of kifunensine as an inhibitor.

Inhibitor Conformations in dGMII and hERMI. The inhibitors kifunensine and 1-deoxymannojirimycin have been shown in the active sites of both dGMII and hERMI. As mentioned, kifunensine adopts a $^{1,4}B$ conformation with a prominent C_1-N kink in dGMII and a $^{1}C_4$ conformation in hERMI.

1-Deoxymannojirimycin is a smaller inhibitor that contains a pyranose ring. This inhibitor is forced into distinct chair

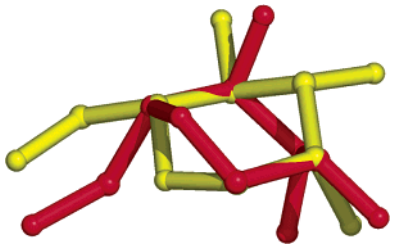

FIGURE 7: Superposition of 1-deoxymannojirimycin from two α-mannosidases: dGMII (yellow) and hERMI (red). It is evident that DMJ adopts two distinct chair conformations in each enzyme: $^4C_1$ in dGMII and $^1C_4$ in hERMI.

conformations in each active site, as seen by a $^4C_1$ conformation in dGMII and a $^1C_4$ conformation in hERMI (Figure 7).

Implications in the Context of the Catalytic Mechanism. There has been significant progress in recent years in defining the conformational states adopted by substrates, transition state analogues, and inhibitors on binding to glycosyl hydrolase catalytic sites, with emphasis primarily (but not exclusively) on retaining β-glycosidases. Recently, Davies et al. (*20*, *21*) have cast these observations into the context of conformational itineraries (*18*) that a saccharide ring undergoes in the process of hydrolysis and have begun to assign the particular itineraries undertaken by various glycosyl hydrolase families.

As that review points out, the $^1C_4$ kifunensine conformation observed in the family 47 inverting hERMI is consistent with this enzyme following a series of conformations passing through a $^3H_4$ transition state during the course of the reaction (*20*). The data presented here on the $^{1,4}B$ structure for kifunensine in dGMII suggest that this family 38 retaining enzyme proceeds via a $B_{2,5}$ transition state. This proposal supports the recent observation of covalent intermediates in dGMII, which suggests that the glycosyl hydrolase family 38 mechanism follows an itinerary opposite to that of the family 26 retaining β-mannanase (*22*). Although the glycosylation steps for both pass through a $B_{2,5}$ transition state, in family 38 the covalent intermediate adopts a $^1S_5$ conformation, while in the case of family 26, this conformation is seen for the Michaelis complex.

As pointed out by Davies et al., the early supposition that glycosyl hydrolases pass through a transition state with a $^4H_3$ configuration has been modified with the accumulation of more data (*20*). The results presented here show that the conformations of common inhibitors in enzymes of different families can shed light on the pathways followed by those enzymes and on their likely transition state configurations. This information is particularly valuable in support of efforts to derive specific inhibitors of glycosidases with medical importance.

ACKNOWLEDGMENT

We would like to thank P. Lynne Howell for helpful discussions. We acknowledge the staff at the Cornell High Energy Synchrotron Source (CHESS) in Ithaca, NY, for their support.

REFERENCES

1. Dennis, J. W., Granovsky, M., and Warren, C. E. (1999) *Bioessays 21*, 412−421.
2. Grünewald, S., Matthijs, G., and Jaeken, J. (2002) *Pediatr. Res. 52*, 618−624.
3. Freeze, H. (2002) *Biochim. Biophys. Acta 1573*, 388−393.
4. Korczak, B., Goss, P., Fernandez, B., Baker, M., and Dennis, J. W. (1994) *Adv. Exp. Med. Biol. 353*, 95−104.
5. Dennis, J. W., Granovsky, M., and Warren, C. E. (1999) *Biochim. Biophys. Acta 1473*(1), 21−34.
6. Roth, J. (2002) *Chem. Rev. 102*, 285−303.
7. Herscovics, A. (1999) *Biochim. Biophys. Acta 1473*, 96−107.
8. Rabouille, C., Kuntz, D. A., Lockyer, A., Watson, R., Signorelli, T., Rose, D. R., van den Heuvel, M., and Roberts, D. B. (1999) *J. Cell Sci. 112*, 3319−3330.
9. van den Elsen, J. M., Kuntz, D. A., and Rose, D. R. (2001) *EMBO J. 20*, 3008−3017.
10. Moremen, K. W. (2002) *Biochim. Biophys. Acta 1573*, 225−235.
11. Heikinheimo, P., Helland, R., Leiros, H. K. S., Leiros, I., Karlsen, S., Evjen, G., Ravelli, R., Schoehn, G., Ruigrok, R., Tollersrud, O. K., McSweeney, S., and Hough, E. (2003) *J. Mol. Biol. 327*, 631−644.
12. Vallee, F., Lipari, F., Yip, P., Sleno, B., Herscovics, A., and Howell, P. L. (2000) *EMBO J. 19*, 581−588.
13. Elbein, A. D., Kerbacher, J. K., Schwartz, C. J., and Sprague, E. A. (1991) *Arch. Biochem. Biophys. 288*, 177−184.
14. Elbein, A. D., Tropea, J. E., Mitchell, M., and Kaushal, G. P. (1990) *J. Biol. Chem. 265*, 15599−15605.
15. Otwinowski, Z., and Minor, W. (1997) *Methods Enzymol. 276*, 307−326.
16. Brunger, A. T., Adams, P. D., Clore, G. M., DeLano, W. L., Gros, P., Grosse-Kunstleve, R. W., Jiang, J. S., Kuszewski, J., Nilges, M., Pannu, N. S., Read, R. J., Rice, L. M., Simonson, T., and Warren, G. L. (1998) *Acta Crystallogr., Sect. D 54*(Pt 5), 905−921.
17. Vallee, F., Karaveg, K., Herscovics, A., Moremen, K. W., and Howell, P. L. (2000) *J. Biol. Chem. 275*, 41287−41298.
18. Stoddart, J. F. (1971) *Stereochemistry of Carbohydrates*, Wiley-Interscience, New York.
19. Lehmann, J. (1998) *Carbohydrates: Structure and Biology*, Thieme, New York.
20. Davies, G. J., Ducros, V. M.-A., Varrot, A., and Zechel, D. L. (2003) *Biochem. Soc. Trans. 31*, 523−527.
21. Ducros, V. M.-A., Zechel, D. L., Murshudov, G. N., Gilbert, H. J., Szabo, L., Stoll, D., Withers, S. G., and Davies, G. J. (2002) *Angew. Chem., Int. Ed. Engl. 41*, 2824−2827.
22. Numao, S., Kuntz, D. A., Withers, S. G., and Rose, D. R. (2003) *J. Biol. Chem.*, in press.

BI034742R